Electronic Supplementary Information for:

Host dependence of the electron affinity of molecular dopants

Jing Li,[1] Ivan Duchemin,[2] Otello Maria Roscioni,[3] Pascal Friederich,[4] Marie Anderson,[5] Enrico Da Como,[5] Gabriele Kociok-Köhn,[6] Wolfgang Wenzel,[4] Claudio Zannoni,[3] David Beljonne,[7] Xavier Blase,[1] and Gabriele D'Avino[1]

[1]*Institut Néel CNRS and Grenoble Alpes University, 25 rue des Martyrs, F-38042 Grenoble, France*

[2]*Grenobles Alpes University, CEA, INAC MEM, L_Sim, F-38000 Grenoble, France*

[3]*Dipartimento di Chimica Industriale "Toso Montanari", Università di Bologna, viale Risorgimento 4, 40136 Bologna, Italy*

[4]*Karlsruhe Institute of Technology, Institute of Nanotechnology Hermann-von-Helmholtz-Platz 1, 76344 Eggenstein-Leopoldshafen, Germany*

[5]*Department of Physics and Centre for Photonics and Photonic Materials, University of Bath, Bath, BA2 7AY, United Kingdom*

[6]*Chemical Characterization and Analysis Facility, University of Bath, Bath, BA2 7AY, United Kingdom*

[7]*Laboratory for the Chemistry of Novel Materials, University of Mons, Place du Parc 20, Mons, BE-7000, Belgium*

(Dated: August 2, 2018)

Contents

I. EXTRAPOLATION OF *GW* QUASIPARTICLE ENERGIES TO THE COMPLETE BASIS SET

GW quasiparticle energies are known to depend on the Gaussian basis set employed in the starting DFT calculations, making accurate calculations expensive. In order to overcome this limitation, we propose an effective extrapolation procedure to target quasiparticle energies in the complete basis set (CBS) limit. Our approach is based on the Dunning's correlation consistent basis sets cc-pVXZ[1] (with $X = 2, 3, 4, 5$) and consists in fitting energy levels with a simple exponential function:

$$E(X) = E_{CBS} - b\, e^{-cX}. \tag{1}$$

Results in Figure 1 provide a robust numerical evidence for the applicability of the proposed formula for several molecules. The effect of the basis augmentation with diffuse functions is addressed in Figure 2.

The present analysis allows us to conclude that:

- A simple interpolation based on two calculations at the cc-pVDZ ($X = 2$) and cc-pVTZ ($X = 3$) (assuming $c = 1$ in Eq. 1, red lines in Fig. 1) predicts with good accuracy (<30 meV) the energy levels explicitly computed with larger ($X > 3$) basis.

- The simple two-point approach described above yields extrapolated energy levels that are within 50 meV from the best possible fit employing data points up to $X = 5$ and augmented basis.

- Significant deviations from $c = 1$ in the fit are obtained only for augmented basis.

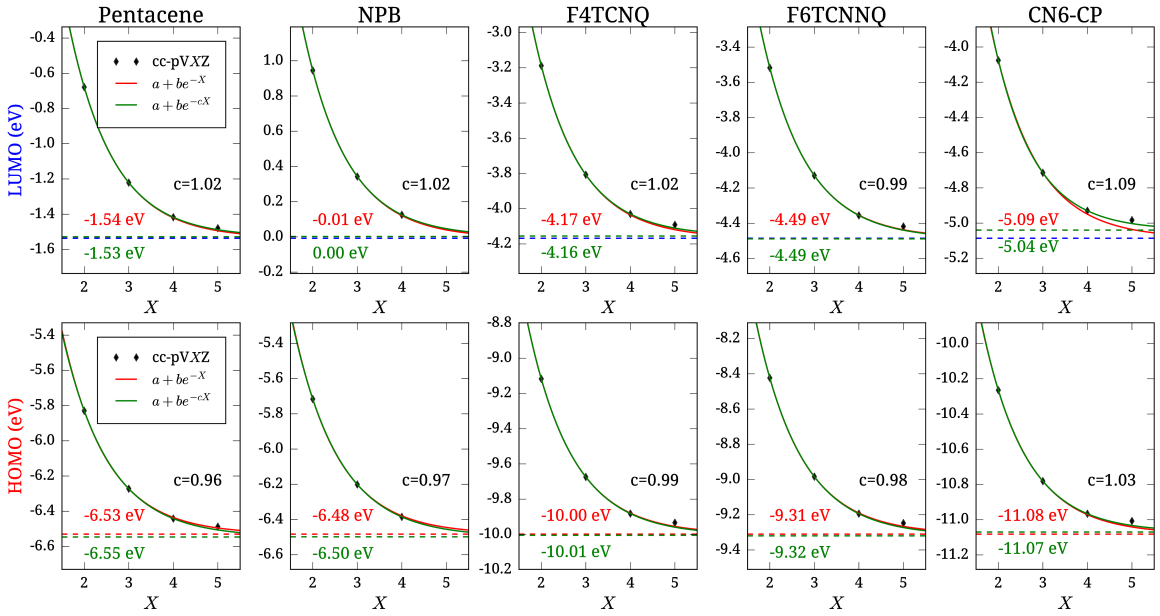

FIG. 1: Dependence of evGW HOMO and LUMO levels on the basis set employed in the DFT calculation. Extrapolation of energy levels to the complete basis set limit is performed via exponential fitting (see legend and text). Extrapolated energy levels (in eV) and the c value obtained from the fit are annotated in the respective panels.

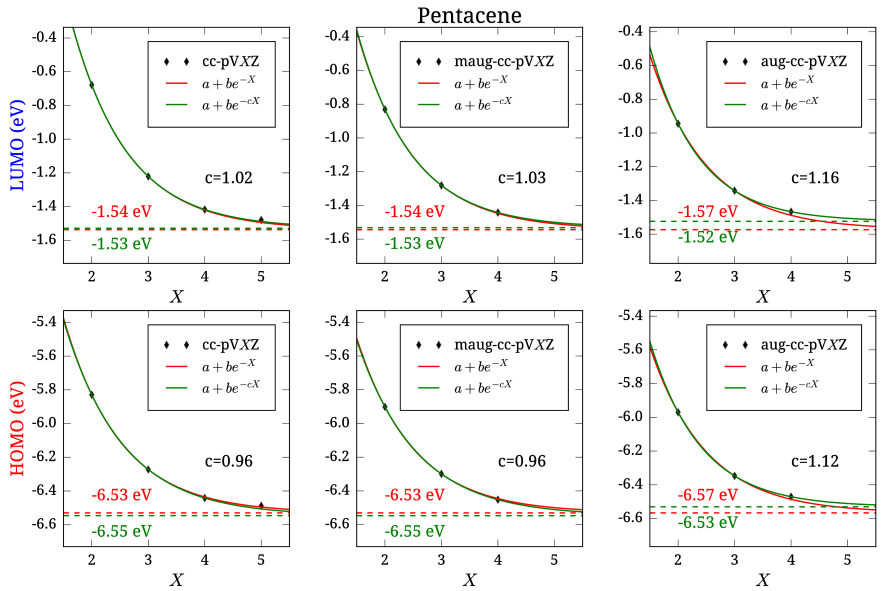

FIG. 2: Effect of basis set augmentation on the basis set dependence of evGW energy levels for pentacene. Extrapolated energy levels (in eV) and the c value obtained from the fit are annotated in the respective panels.

II. BAND STRUCTURE OF F4TCNQ, F6TCNNQ AND NPB

We have performed band structure calculations in order to assess the effect of band dispersion on the IP and EA of pure materials. All-electron band structure calculations were performed at the DFT level (PBE0 functional, 6-31G* Gaussian basis) with the CRYSTAL14 code.[2] Band structure and density of states (DOS) for F4TCNQ, F6TCNNQ and NPB are shown in Figs. 3, 4 and 5, respectively. The labeling of the high-symmetry points of the Brillouin zone follows the conventions given in Ref. 3.

Following Ref. 4, IP and EA including finite band with effects are computed as:

$$\mathrm{IP} = \mathrm{IP}_0 + \delta_v \tag{2}$$

$$\mathrm{EA} = \mathrm{EA}_0 + \delta_c \tag{3}$$

$$\tag{4}$$

where IP_0 and EA_0 refer to charged excitations localized on a single molecule, as obtained from embedded GW calculations. δ_v (δ_c) is the contribution from band dispersion, calculated as the energy difference between the top (bottom) of the valence (conduction) band and the band centroid $E_0 = \int En(E)\,dE / \int n(E)dE$, where $n(E)$ is the band DOS.

The total bandwidth and the corresponding shifts in IP and EA are given in Table I.

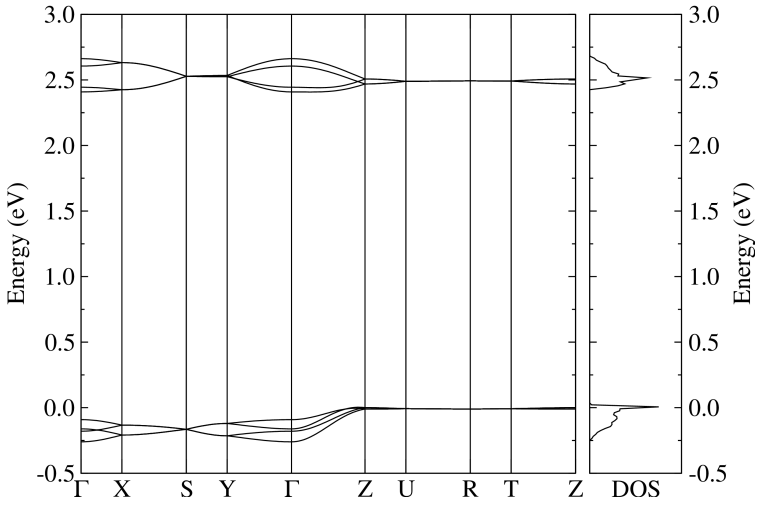

FIG. 3: Electronic band structure and density of states (DOS) of F4TCNQ.

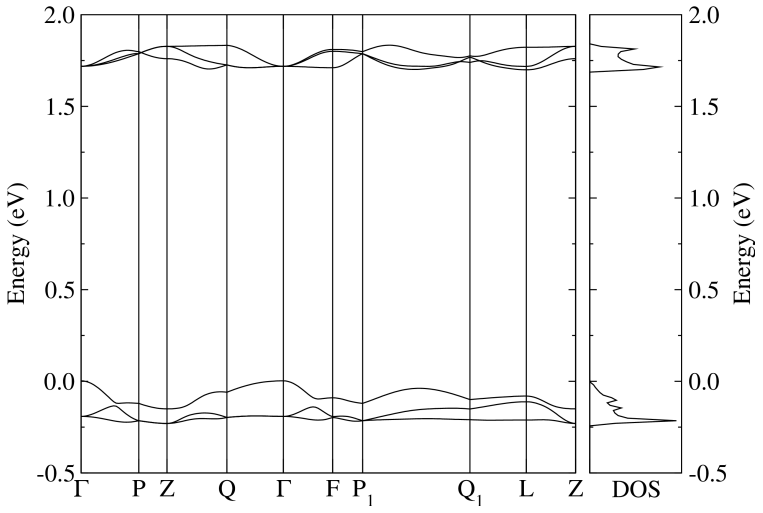

FIG. 4: Electronic band structure and density of states (DOS) of F6TCNNQ.

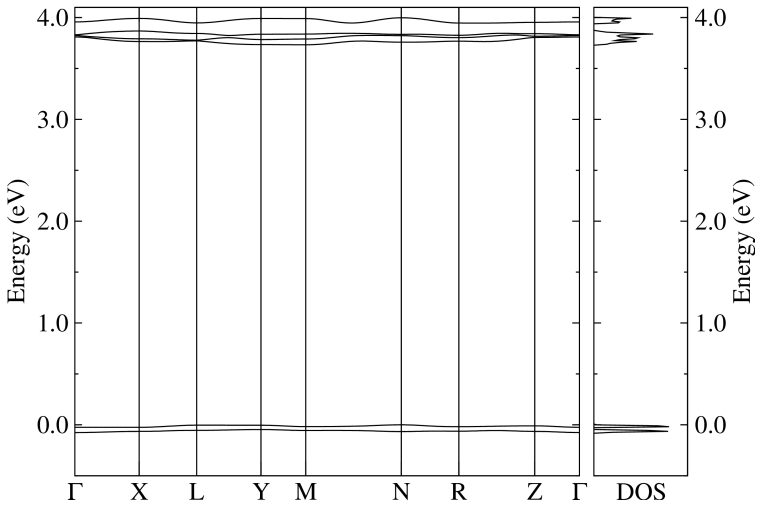

FIG. 5: Electronic band structure and density of states (DOS) of NPB.

system	W_v	δ_v	W_c	δ_c
F4TCNQ	0.27	-0.10	0.26	0.10
F6TCNNQ	0.24	-0.16	0.14	0.06
NPB	0.08	-0.04	0.27	0.11
pentacene	0.64	-0.26	0.76	0.31

TABLE I: Valence/conduction bandwidth (W_v/W_c) and IP/EA shifts (δ_v/δ_c) due to dispersion in eV units. Results from band-structure calculations in Figs. 3, 4 and 5, except for pentacene whose data are from Ref. 4.

III. CRYSTAL STRUCTURE OF F6TCNNQ

F6TCNNQ crystals were obtained by slow evaporation of a saturated solution in acetonitrile. Crystals of suitable size for X-ray diffractometry were isolated and mounted on an Agilent SuperNova-E Dual diffractometer equipped with an Oxford Cryosystem, using CuKα radiation ($\lambda = 1.5418$ Å). Data were processed using the CrysAlisPro software (CrysAlisPro 1.171.38.46, Rigaku Oxford Diffraction, 2015) and analysed using Mercury. The structural data reported below were obtained with the F6TCNNQ crystal at 150 K. F6TCNNQ crystallizes in the R-3 space group with 9 molecules per unit cell, $Z = 9$. The rather high number of molecules per unit cell gives the cell parameters: $a = b = 17.533(4)$ Å, $c = 17.484(3)$ Å. The refined structure, shown in Figure 6, presents orientational disorder of the F6TCNNQ molecules. Such disorder has not been taken into account in electronic structure calculations that considered only one of the possible molecular orientations (red molecules in Fig. 6).

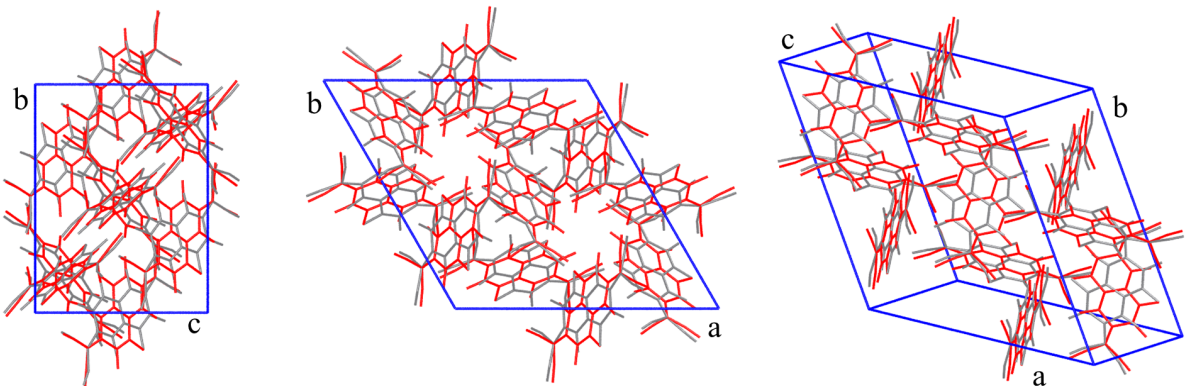

FIG. 6: Molecular packing in the F6TCNNQ crystal, viewed from the a (left) and c (middle) crystal axes and in perspective (right). The two molecular orientations resolved in the refinement of X-ray diffraction data are shown in red and gray, respectively.

IV. ELECTROSTATIC CONTRIBUTION TO ENERGY LEVELS: COMPILATION OF LITERATURE DATA

Electrostatic modelling of several molecular crystals have shown the existence of a correlation between the sign of the electrostatic contribution to the energy levels (Δ_E) and the electrostatic layout of the molecule. Note that different conventions may apply to the sign of Δ_E, here we assume that positive (negative) values increase (decrease) IP and EA.

Table II provides a compilation of literature data for hole transporting materials. For all the materials discussed here, whose electrostatic layout is characterized by electron-rich π cores, negative values of Δ_E were found. Electron transporting semiconductors and p-type dopants do usually feature electron attracting side groups (e.g. cyano group or halogens that are generally introduced to increase the EA) and electron-poor cores, resulting in an opposite electrostatic layout with respect to hole transporting materials. All these systems present positive values of Δ_E, as reported in Table III.

The Δ_E values for pentacene, NPB, F4TCNNQ and F6TCNNQ reported in this work are in line with the above mentioned systematic dependence of electrostatic shift on the electrostatic molecular layout.

system	Δ_E	Ref.	notes
anthracene	-0.12	5	bulk
	-0.13	6	bulk
	-0.25	7,8	bulk
pentacene	-0.10	4	bulk
	-0.12	6	bulk
	-0.12	5	bulk
	-0.32	4	surface (001)
	-0.34	9	surface (001)
	-0.4†	10	surface, short-edge-on
	-0.78†	11	surface (001)
quaterthiophene	-0.15	5	bulk
sexithiophene	-0.16	5	bulk
sexithiophene	-0.4†	10	surface, short-edge-on
ZnPC	-0.8†	12	surface, edge-on
ZnPC	-0.4†	10	surface

TABLE II: Compilation of literature data of electrostatic contribution to charge transport levels Δ_E (eV units) for different hole transporting molecular semiconductors. In order to avoid issues arising from different possible partitioning of the environmental contribution to energy levels, the data in the present table are defined as $\Delta_E = (P^+ - P^-)/2$, where $P^+ = IP - IP_{gas}$ and $P^- = EA_{gas} - EA$, except for data marked with † for which we report the values of electrostatic term as given in the corresponding reference.

system	Δ_E	Ref.	notes
perfluoropentacene	0.34	4	bulk
	0.39	6	bulk
	0.65	4	(100) surface
	0.61	9	(100) surface
	1.05†	11	(100) surface
F_4ZnPC	0.2†	12	surface, edge-on
F_8ZnPC	1.0†	12	surface, edge-on
F_{16}ZnPC	1.1†	12	surface, edge-on
PTCDA	1.19	7,8	bulk
F-PDI-Cl_2	0.48	5	bulk
D5M	1.55†	10	surface, short-edge-on

TABLE III: Compilation of literature data of electrostatic contribution to charge transport levels Δ_E (eV units) for different electron transporting molecular semiconductors, presenting the same electrostatic layout of p-type dopants. In order to avoid issues arising from different possible partitioning of the environmental contribution to energy levels, the data in the present table are defined as $\Delta_E = (P^+ - P^-)/2$, where $P^+ = IP - IP_{gas}$ and $P^- = EA_{gas} - EA$, except for data marked with † for which we report the values of electrostatic term as given in the corresponding reference.

V. AMORPHOUS F6TCNNQ-DOPED NPB: MORPHOLOGY SIMULATIONS

Amorphous morphologies of pristine NPB and NPB doped with F6TNNQ (at 2, 5 and 10% molar concentration) were generated using the Monte Carlo based simulated annealing protocol DEPOSIT.[13] To mimic the vapor deposition process, the molecules are added to a simulation box sequentially. Each of the molecules is annealed from 4000 K to 300 K in 140000 Monte Carlo steps. This annealing procedure is repeated 10 times for each molecule. The energies are evaluated using a classical force field in which the internal degrees of freedom of the molecules are reduced to rotations of dihedral angles. Molecule specific dihedral potentials derived using DFT (B3LYP/def2-SV(P) level) based parametrization procedure. Intermolecular energies are evaluated using Lennard-Jones potentials between the atoms, plus electrostatic interactions based on DFT derived partial charges. Each morphology contained 1050 molecules with periodic boundary conditions in the x and y directions (9 nm box size). There are no periodic boundary conditions in growth direction (z direction).

After completing the deposition, the pristine and doped samples have been equilibrated at room temperature with atomistic molecular dynamics (MD) simulations. Periodic boundary conditions were imposed in three dimensions, in order to convert the film obtained upon deposition into an amorphous bulk. MD simulations were carried out at a constant pressure of 1 bar and temperature 300 K (NPT ensemble) with damping constants of 2 and 0.2 picoseconds, respectively.

MD simulations were carried out with the program LAMMPS[14,15], version 11May16. The force field employed in the simulations was obtained from the online repository Advanced Topology Builder (ATB), version 2.2[16–18]. Minor changes were made on the molecular topologies obtained from the ATB repository: namely, exclusion bonds were removed between aromatic moieties connected by single bonds (e.g. in tertiary amines)[18,19]. The amended GROMOS-ATB force field was then used in conjunction with the program MOLTEMPLATE[20,21] to generate the input files required to carry out the MD simulations.

The samples were equilibrated for 5 ns, followed by other 5 ns of production run used to compute electronic properties. No evidence for dopant solid-state diffusion has been observed in the time span of MD simulations. The densities of the four MD-simulated samples are reported in Table IV.

doping	density (g/cm^3)
0 %	1.07
2 %	1.12
5 %	1.13
10%	1.14
0 % (crystal)	1.22

TABLE IV: Densities of the amorphous MD-simulated amorphous pristine and doped samples. Doping load is given in % molar concentration. For comparison we report the experimental density of the NPB crystal from x-ray diffraction.[22]

VI. AMORPHOUS F6TCNNQ-DOPED NPB: ELECTRONIC PROPERTIES

We performed extensive electronic structure calculations for MD-simulated amorphous morphologies of pristine NPB and doped with F6TCNNQ at 2, 5 and 10% concentration. In order to sample IP and EA over disordered morphology we apply a computational strategy combining *GW*, DFT and CR calculations. The energy of localized holes on NPB and electrons on F6TCNNQ read:

$$\mathrm{IP} = \mathrm{IP}_g + P^+ \tag{5}$$

$$\mathrm{EA} = \mathrm{EA}_g - P^- \tag{6}$$

where IP_g and EA_g are evaluated as total energy differences between charged and neutral species (ΔSCF scheme) at the PBE0/SVP level of theory in the gas phase. The ΔSCF results at the crystal structure geometry, $\mathrm{IP}_g = 6.04$ eV and $\mathrm{EA}_g = 4.18$ eV, are in line with the reference evGW values of 6.50 and 4.49 eV, respectively. The IP_g and EA_g values presented in the following are corrected for the difference to evGW levels, so that DFT only accounts for the variation of the levels with the molecular conformation, while for absolute values we rely on accurate *GW* calculations. The polarization energies, P^+ and P^-, account for the electrostatic interaction of the charge with the polarizable environment and are evaluated with self-consistent CR calculations, extrapolated for an infinite bulk. The CR model is parametrized with molecular polarizability from DFT (PBE0/6-311++G**) and semiempirical (ZINDO) atom-atom polarizability tensor. Atomic charges of neutral and charged molecules from electrostatic potential fitting were obtained at the DFT level (PBE0/SVP) for each molecule in the MD sample at its specific geometry. Electronic structure calculations to sample energetic properties on amorphous morphologies and to parametrize the CR model were performed with the ORCA v4.0 code.[23]

The results of our statistics over IP and EA gathered over one snapshot of MD trajectory are reported in Figure 7 and Table V. These results show that conformational and electrostatic disorder largely affects the energetics of charge carriers, especially the EA of F6TCNNQ. We notice that the gap between the center of IP and EA distribution (Figure 7, left panels) is rather large (∼0.8 eV), yet the spread of the distributions is considerable. The distributions and mean values of IP and EA are weakly dependent on the doping load.

The electron-hole binding energy V_{eh} of ion pair states is calculated as the sum of screened

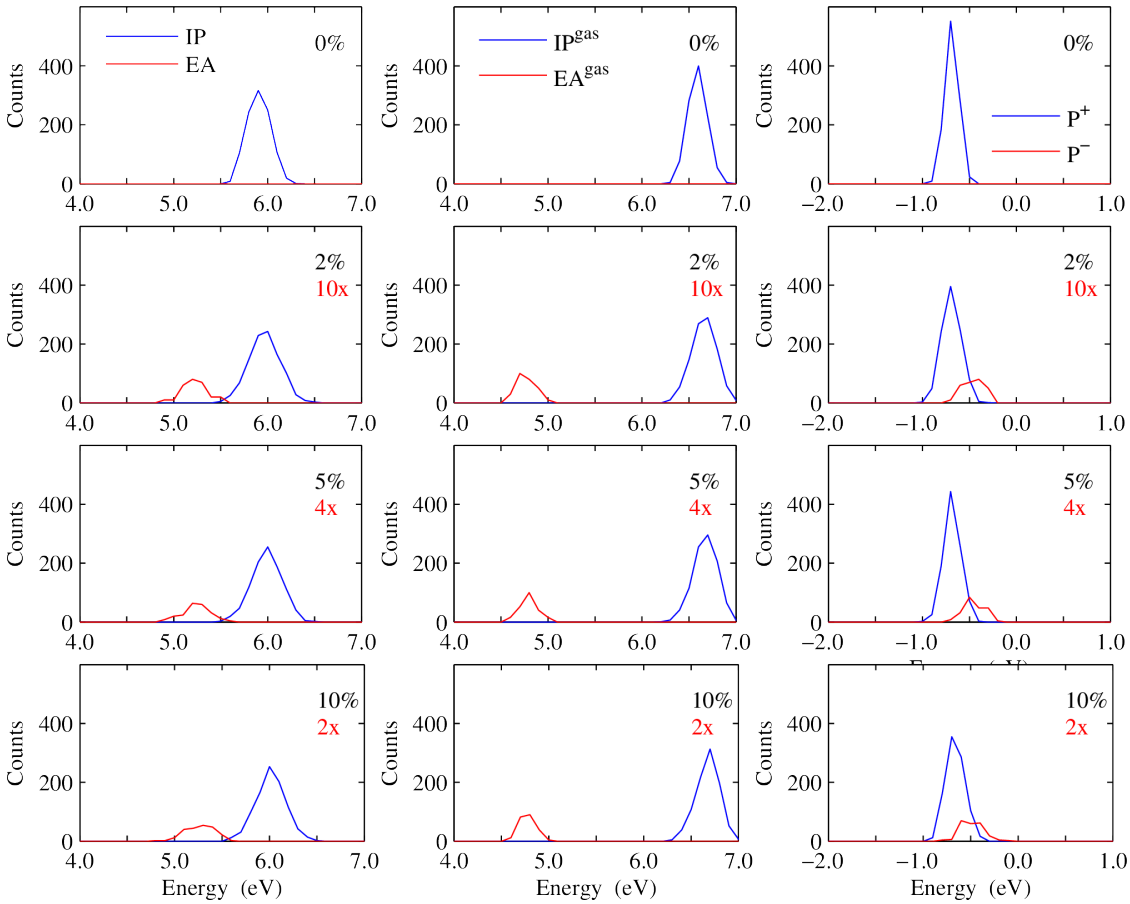

FIG. 7: Distribution of of IP (EA) of NPB (F6TCNNQ) molecules in the amorphous MD samples (left column). Intramolecular (gas-phase) and intermolecular contributions (polarization energy P) to IP and EA are shown in the central and right-hand column, respectively. F6TCNNQ doping load increases row-wise.

doping	IP	EA	IP_g	EA_g	P^+	P^-
0 %	5.90 ±0.12	-	6.59 ±0.10	-	-0.69 ±0.07	-
2 %	5.97 ±0.17	5.21 ±0.13	6.66 ±0.13	4.76 ±0.10	-0.69 ±0.10	-0.46 ±0.11
5 %	5.99 ±0.16	5.24 ±0.15	6.67 ±0.13	4.79 ±0.10	-0.68 ±0.09	-0.45 ±0.11
10 %	6.01 ±0.15	5.26 ±0.15	6.67 ±0.12	4.78 ±0.08	-0.66 ±0.10	-0.49 ±0.12

TABLE V: Mean values and standard deviations of IP (EA) of NPB (F6TCNNQ) molecules in the amorphous MD samples of different doping load. IP and EA are partitioned into intramolecular (gas-phase) and intermolecular contributions (polarization energy P). Energies are in eV.

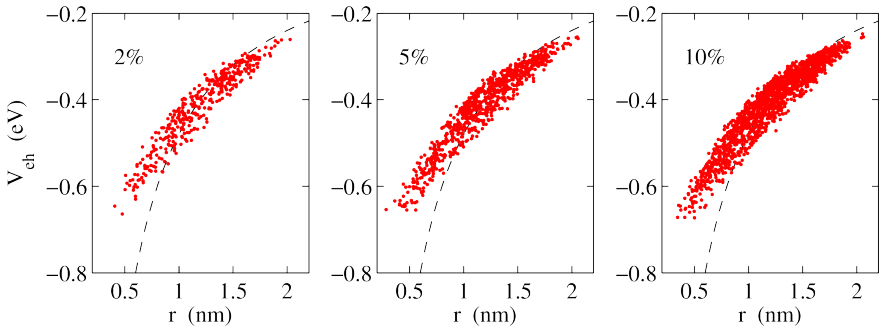

FIG. 8: Electron-hole binding energy as a function of the NPB-F6TCNNQ distance in the amorphous MD samples. Red points correspond to atomistic calculations (screened Coulomb interaction between atomic charges), the black line is a screened Coulomb potential between point charges. The dielectric constant is set to $\varepsilon_r = 3$.

pairwise Coulomb interactions between point atomic charges:

$$V_{eh} = \frac{1}{\varepsilon_r} \sum_{i,j} \frac{\delta q_i^h \, \delta q_j^e}{r_{ij}} \tag{7}$$

where $\delta q_i^{h/e}$ is the difference between the atomic charges in the charged and in the neutral state of molecule i. A previous study on F4TCNQ-doped pentacene showed that the screened Coulomb approximation leads to very good results compared to much more expensive self-consistent calculations.[24]

Figure 8 shows V_{eh} as a function of the distance between hole and electron centroids of nearest-neighbors NPB-F6TCNNQ dimers in the MD samples (red points). V_{eh} approximately follow a screened Coulomb potential between point unit charges (dashed line) at large distance, but it substantially deviates at shorter ones, where the molecular size and conformation affect the intermolecular interaction.

We are finally in the position to discuss the possibility for dopant ionization. We consider a dopant to be ionized at room temperature if it is energetically possible to transfer an electron to one of its neighboring host molecules, i.e. the energy of the corresponding charge transfer state is lower than 50 meV. Table VI presents the fraction of ionized dopants χ in the MD samples of different doping load. We consider the effect of structural relaxation upon charging (polaronic effects, by comparing results obtained with the vertical and adiabatic IP and EA), as well as the impact of the medium dielectric constant. We conclude that almost all F6TCNNQ dopants can ionize in NPB and that the intramolecular relaxation energy is

doping	$\chi^a(\epsilon_r = 3)$	$\chi^v(\epsilon_r = 3)$	$\chi^v(\epsilon_r = 2)$	$\chi^v(\epsilon_r = 1)$
2	96	33	89	100
5	95	43	91	100
10	94	43	89	100

TABLE VI: Percentage of dopants χ that can ionize at room temperature as a function of the doping load and of the medium dielectric constant ϵ_r. χ^v and χ^a are computed assuming the vertical and adiabatic gap, respectively. The intramolecular relaxation energy ($\lambda = \lambda^+ + \lambda^- = 150 + 134 = 284$ meV, PBE0/def2-SVP level), turns out to be determinant for the ionization.

determinant for an efficient and quantitative ionization of the dopants. We remark that the present analysis is valid in the limit of one dopant ionized at a time. In the case of multiple ionized dopants, the dipole fields of electron-hole pairs add to the electrostatic disorder of neutral molecules, leading to a further increase of the fraction of ionized dopants.

[1] T. H. Dunning, J. Chem. Phys. **90**, 1007 (1989).

[2] R. Dovesi, R. Orlando, A. Erba, C. M. Zicovich-Wilson, B. Civalleri, S. Casassa, L. Maschio, M. Ferrabone, M. De La Pierre, P. D'Arco, et al., Int. J. Quantum Chem. **114**, 1287 (2014).

[3] W. Setyawan and S. Curtarolo, Comput. Mater. Sci. **49**, 299 (2010).

[4] J. Li, G. D'Avino, I. Duchemin, D. Beljonne, and X. Blase, Phys. Rev. B **97**, 035108 (2018).

[5] G. D'Avino, L. Muccioli, C. Zannoni, D. Beljonne, and Z. G. Soos, J. Chem. Theory Comput. **10**, 4959 (2014).

[6] S. M. Ryno, S. R. Lee, J. S. Sears, C. Risko, and J.-L. Brédas, J. Phys. Chem. C **117**, 13853 (2013).

[7] E. V. Tsiper and Z. G. Soos, Phys. Rev. B **64**, 195124 (2001).

[8] J. M. Sin, E. V. Tsiper, and Z. G. Soos, Europhys. Lett. **60**, 743 (2002).

[9] H. Yoshida, K. Yamada, J. Tsutsumi, and N. Sato, Phys. Rev. B **92**, 075145 (2015).

[10] C. Poelking and D. Andrienko, J. Chem. Theory Comput. **12**, 4516 (2016).

[11] B. J. Topham and Z. G. Soos, Phys. Rev. B **84**, 165405 (2011).

[12] M. Schwarze, W. Tress, B. Beyer, F. Gao, R. Scholz, C. Poelking, K. Ortstein, A. A. Gunther,

D. Kasemann, D. Andrienko, et al., Science **352**, 1446 (2016).

[13] T. Neumann, D. Danilov, C. Lennartz, and W. Wenzel, J. Comput. Chem. **34**, 2716 (2013).

[14] S. Plimpton, J. Comput. Phys. **117**, 1 (1995).

[15] *Lammps molecular dynamics simulator*, `http://lammps.sandia.gov`.

[16] A. K. Malde, L. Zuo, M. Breeze, M. Stroet, D. Poger, P. C. Nair, C. Oostenbrink, and A. E. Mark, J. Chem. Theory Comput. **7**, 4026 (2011).

[17] S. Canzar, M. El-Kebir, R. Pool, K. Elbassioni, A. K. Malde, A. E. Mark, D. P. Geerke, L. Stougie, and G. W. Klau, J. Comput. Biol. **20**, 188 (2013).

[18] K. B. Koziara, M. Stroet, A. K. Malde, and A. E. Mark, J. Comput. Aided Mol. Des. **28**, 221 (2014).

[19] C. Oostenbrink, A. Villa, A. E. Mark, and W. F. Van Gunsteren, J. Comput. Chem. **25**, 1656 (2004).

[20] A. I. Jewett, Z. Zhuang, and J. Shea, Biophys. J. **104**, 169a (2013).

[21] *Moltemplate*, `http://www.moltemplate.org`.

[22] J.-A. Cheng and P.-J. Cheng, J. Chem. Crystallogr. **40**, 557 (2010).

[23] F. Neese, WIREs Comput. Mol. Sci. **2**, 73 (2012).

[24] J. Li, G. D'Avino, A. Pershin, D. Jacquemin, I. Duchemin, D. Beljonne, and X. Blase, Phys. Rev. Mater. **1**, 025602 (2017).